IOPscience iopscience.iop.org

Home Search Collections Journals About Contact us My IOPscience

The structural and optical characterization of a new class of dilute nitride compound semiconductors: GaInNP

This article has been downloaded from IOPscience. Please scroll down to see the full text article.

2004 J. Phys.: Condens. Matter 16 S3245

(http://iopscience.iop.org/0953-8984/16/31/018)

View the table of contents for this issue, or go to the journal homepage for more

Download details:
IP Address: 129.252.86.83
The article was downloaded on 27/05/2010 at 16:22

Please note that terms and conditions apply.

INSTITUTE OF PHYSICS PUBLISHING JOURNAL OF PHYSICS: CONDENSED MATTER

J. Phys.: Condens. Matter **16** (2004) S3245–S3256 PII: S0953-8984(04)74053-9

The structural and optical characterization of a new class of dilute nitride compound semiconductors: GaInNP

H P Hsu[1], **Y S Huang**[1,5], **C H Wu**[2], **Y K Su**[2], **F S Juang**[3], **Y G Hong**[4] **and C W Tu**[4]

[1] Department of Electronic Engineering, National Taiwan University of Science and Technology, Taipei 106, Taiwan
[3] Institute of Microelectronics, Department of Electrical Engineering, National Cheng Kung University, Tainan 701, Taiwan
[2] Department of Electro-Optics Engineering, National Huwei Institute of Technology, Yunlin 632, Taiwan
[4] Department of Electrical and Computer Engineering, University of California, San Diego, La Jolla, CA 92093-0407, USA

Received 7 January 2004
Published 23 July 2004
Online at stacks.iop.org/JPhysCM/16/S3245
doi:10.1088/0953-8984/16/31/018

Abstract

We report a detailed structural and optical characterization of $Ga_{0.46}In_{0.54}N_xP_{1-x}$ ($0 \leqslant x \leqslant 2\%$) films grown by gas-source molecular beam epitaxy on GaAs(001) substrates. The polarized high resolution x-ray rocking curves (HXRC) and contactless electroreflectance (CER) and piezoreflectance (PzR) spectra at room temperature show anisotropic character along the [110] and $[1\bar{1}0]$ directions. Ordering-induced superlattice-like microstructure observed in high resolution transmission electron microscope (HTEM) images confirms the spontaneous ordering in $Ga_{0.46}In_{0.54}N_xP_{1-x}$ layers. In addition, the temperature dependent optical properties are characterized via polarized PzR measurements in the range between 15 and 300 K. The PzR spectra obtained are fitted using the first derivative of a Lorentzian line-shape functional form. The valence band maximum, crystal field/strain splitting and spin–orbit splitting to conduction band transition energies, denoted respectively as E_g, $E_g + \Delta_{12}$ and $E_g + \Delta_{13}$, are accurately determined. The temperature dependences of these near band edge critical point transition energies are analysed using the Varshni expression and an expression containing the Bose–Einstein occupation factor for phonons. The parameters that describe the temperature variation of the transition energies are evaluated and discussed.

[5] Author to whom any correspondence should be addressed.

1. Introduction

Recently, the $Ga_{0.52}In_{0.48}P$ grown lattice matched to GaAs has received considerable attention due to its potential applications in optoelectronic and electronic devices, such as semiconductor lasers [1, 2], heterojunction bipolar transistors (HBT) [3, 4] and high efficiency tandem solar cells [5]. GaInP/GaAs structures have several significant advantages over AlGaAs/GaAs structures, such as larger valence band discontinuity, better etch selectivity and lesser oxidation effect.

Spontaneous ordering in $Ga_{0.52}In_{0.48}P$ has been widely investigated in recent years [6–8]. Depending on its growth conditions, $Ga_{0.52}In_{0.48}P$ can be grown on GaAs substrates in an orderly or disorderly fashion [9], which results in the discrepancy of the band gap energy. The ordering phenomenon in such compounds is a very important property, which will induce changes in the electronic and optical properties of the material.

There is much interest in III–N–V compound semiconductors [10–12], because only a small amount of nitrogen incorporation in conventional GaAs and InP-based III–V compounds results in a very large band gap bowing, with the majority of the reduction resulting from the lowering of the conduction band. Naturally, we expect a similar effect in $Ga_{1-x}In_xN_yP_{1-y}$, thus making it a suitable material for use as the emitter or collector of an n–p–n HBT—specifically, the tunnel–collector HBT since the conduction band offset could be made to be zero [13]. The large valence band discontinuity and large hole effective mass would block holes, while there would be no electron barriers at the base–collector junction. Despite its possible applications, to date there have been few reports on nitrogen incorporated in $Ga_{1-x}In_xP$ [14, 15].

In this paper, we report a detailed structural and optical study on four $Ga_{0.46}In_{0.54}N_xP_{1-x}$ (x from 0 to 0.02) epilayers grown on GaAs(001) by gas-source molecular beam epitaxy (GSMBE). The anisotropic properties along the [110] and $[1\bar{1}0]$ directions are characterized by the polarized high resolution x-ray rocking curves (HXRC) and contactless electroreflectance (CER) and piezoreflectance (PzR) spectra. The temperature dependent optical properties are studied via the polarized PzR measurements in the range between 15 and 300 K. The near band edge critical point transition energies are determined and their temperature dependences are analysed using the Varshni expression [16] and an expression containing the Bose–Einstein occupation factor for phonons [17, 18]. The parameters that describe the temperature variations of the transition energies are evaluated and discussed.

2. Experimental detail

All the samples used in this study were grown on GaAs(100) semi-insulating substrates by GSMBE using elemental gallium (Ga) and indium (In), thermally cracked arsine (AH_3) and phosphine (PH_3), and a RF plasma nitrogen radical beam source. After removing the surface oxide from the GaAs substrate at 620 °C under As_2 flux, a 1000 Å thick buffer GaAs layer was grown. The substrate temperature was then lowered to the growth temperature which was controlled between 380 and 480 °C and the nitrogen plasma was ignited. Growth was monitored by reflection high energy electron diffraction (RHEED). Four undoped 2350 Å thick $Ga_{0.46}In_{0.54}N_xP_{1-x}$ layers (A, B, C and D) with different N concentrations were grown for this study. The indium composition was determined by dynamical theory simulations of the recorded XRC for the GaInP calibration sample. Assuming that nitrogen incorporation does not affect indium composition, the nitrogen contents for samples A, B, C and D were then estimated to be 0, 0.5%, 1% and 2%, respectively. The HXRC measurement was performed using a Bede x-ray diffractometer. Photoluminescence (PL) was carried out at room temperature by using the 514.5 nm line of an Ar ion laser as the excitation source.

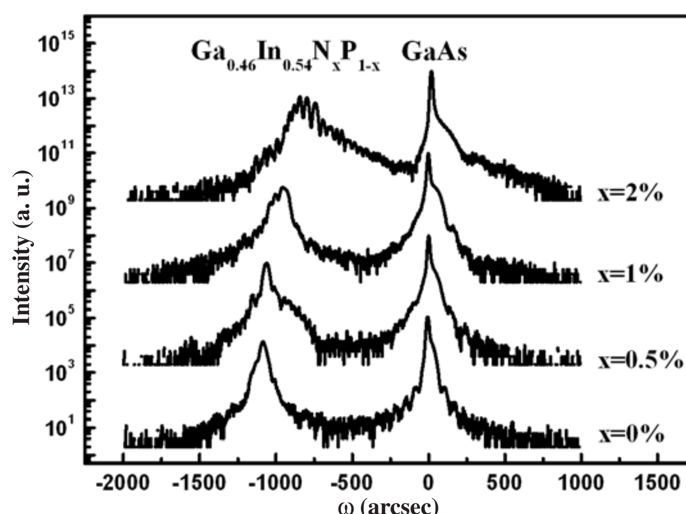

Figure 1. High resolution x-ray rocking curves of $Ga_{0.46}In_{0.54}N_xP_{1-x}$ epilayers with nitrogen content $x = 0$, 0.5%, 1% and 2%.

CER utilized a condenser-like system consisting of a front wire grid electrode with a second metal electrode separated from the first electrode by insulating spacers, which were ~0.1 mm larger than the sample thickness. The sample was placed between these two capacitor plates. Thus, there was nothing in direct contact with the front surface of the sample. The probe beam was incident through the front wire grid. Electromodulation was achieved by applying an ac voltage (1 kV peak to peak at 200 Hz) across the electrodes. The PzR measurements were achieved by gluing the thin sample on a 0.15 cm thick lead zirconate titanate (PZT) piezoelectric transducer driven by a 300 V_{rms} sinusoidal wave at 200 Hz. In order to enhance the modulation effects, the substrate of the sample was polished with successively finer grades of silicon carbide grinding paper to a thickness of about 100 μm. A 150 W tungsten–halogen lamp filtered by a PTI 0.25 m monochromator provided the monochromatic light. The reflected light was detected by an EG&G type HUV-2000 B silicon photodiode, and the signal was recorded from a Perkin-Elmer 7265 DSP lock-in amplifier. Oriel visible–near infrared dichroic linear polarizers were employed for polarization dependent measurements. An RMC model 22 closed-cycle cryogenic refrigerator equipped with a model 4075 digital thermometer controller was used for low temperature measurements. The measurements were made between 15 and 300 K with a temperature stability of 0.5 K or better.

3. Results and discussion

Figure 1 shows the HXRC of $Ga_{0.46}In_{0.54}N_xP_{1-x}$ epilayers with $x = 0, 0.5\%, 1\%$ and 2%. The HXRC of $Ga_{0.46}In_{0.54}P$ shows 0.42% lattice mismatch to the GaAs substrate. With nitrogen incorporation, the peak of $Ga_{0.46}In_{0.54}N_xP_{1-x}$ moves toward the peak of GaAs, indicating that the mismatch between the epilayer and GaAs substrate has decreased. However, the epitaxial quality becomes poorer for samples with nitrogen incorporation. For the sample with nitrogen content equal to 2%, the splitting features of the XRC reveal a poorer quality of the layer. Figure 2 depicts the room temperature PL spectra of samples A, B and C with the peak positions located at 1.826, 1.784 and 1.745 eV, respectively. With nitrogen incorporation the

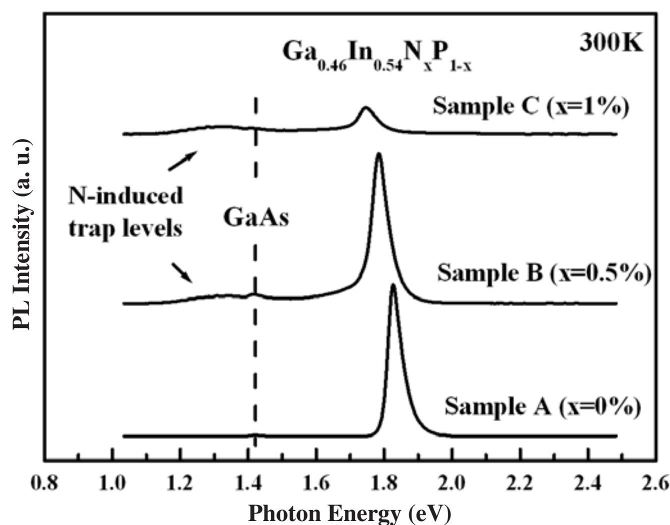

Figure 2. Room temperature photoluminescence spectra of $Ga_{0.46}In_{0.54}N_xP_{1-x}$ epilayers with nitrogen content $x = 0$, 0.5% and 1%.

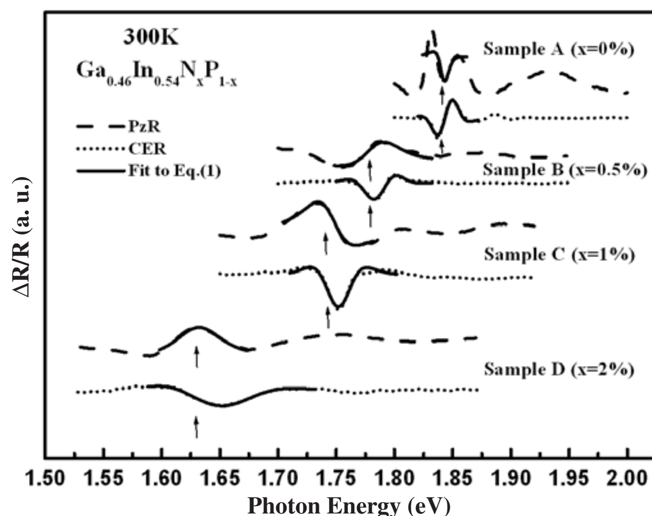

Figure 3. Room temperature CER and PzR spectra of $Ga_{0.46}In_{0.54}N_xP_{1-x}$ epilayers with nitrogen content $x = 0$, 0.5%, 1% and 2% in the vicinity of the band edge. The energies of the band gaps obtained from the fits are indicated by arrows.

PL intensity decreases and the full width at half-maximum (FWHM) increases due to the alloy scattering. The long tail on the lower energy side observed in PL spectra of samples B and C shows the probable effect of the nitrogen-induced trap levels including nitrogen isolated centres, nitrogen pairs and clusters in the samples. With 2% nitrogen content (sample D), no detectable room temperature PL was obtained, indicating the presence of a rather high concentration of nonradiative centres.

Figure 3 shows room temperature CER and PzR spectra for the four $Ga_{0.46}In_{0.54}N_xP_{1-x}$ samples. The dashed and dotted curves represent the experimental CER and PzR spectra,

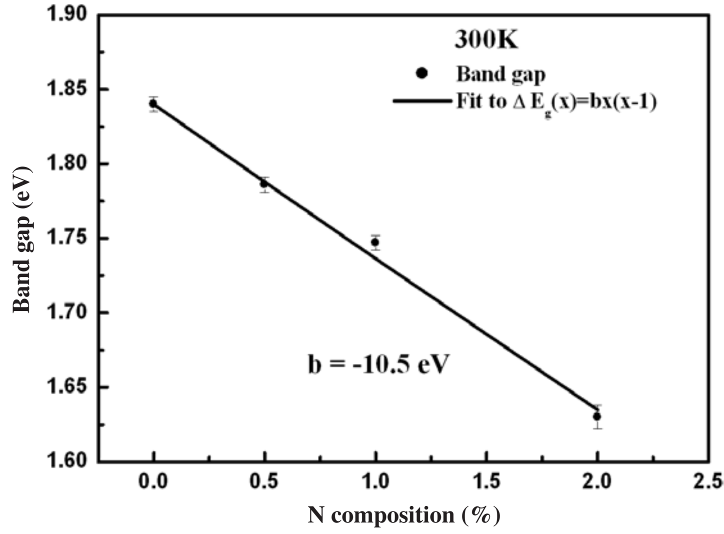

Figure 4. Room temperature energy gaps for $Ga_{0.46}In_{0.54}N_xP_{1-x}$ samples with different nitrogen concentrations.

respectively, and the full curves are the least-squares fits to the line-shape function in the vicinity of the band edge. The functional form used in the fitting procedure corresponds to a first-derivative Lorentzian line-shape function of the form [19]

$$\frac{\Delta R}{R} = \mathrm{Re}\sum_{j=1}^{m} A_j e^{i\theta_j}(E - E_j + i\Gamma)^{-n} \quad (1)$$

where m is the number of critical points, A_j and θ_j are the amplitude and phase of the line shape, E_j and Γ_j are the energy and broadening parameter of the transitions and the value of n depends on the origin of the transitions. For the first-derivative functional form, $n = 2$ is appropriate for the excitonic transitions. The energies of the band gaps obtained from the fits are indicated by arrows. As shown in figure 3, with nitrogen incorporation the linewidth increases due to alloy scattering and the red-shift of the CER and PzR features indicates band gap reduction. Figure 4 shows the decreases of the band gap at room temperature of the four samples with increasing nitrogen content. It is well known that the incorporation of a small amount of nitrogen in III–V semiconductors such as InP [20], GaP [21] and GaAs [22] results in a strong reduction of the band gap in those materials. This behaviour is usually well described by the quadratic correction $\Delta E_g(x) = bx(x-1)$ with b the bowing coefficient. The bowing coefficient obtained $b = -10.5$ eV is found to be smaller than the corresponding values associated with the incorporation of nitrogen in InP ($b = -16$ eV) [20] or GaP ($b = -14$ eV) [21]. However, there is a large uncertainty in this number due to the limited composition range available at the present study.

Figure 5 shows the room temperature CER and PzR spectra of the samples with nitrogen contents $x = 0$, 0.5% and 1% for $\mathbf{E} \parallel [110]$ and $\mathbf{E} \parallel [1\bar{1}0]$ polarizations. The features near the band edge show strong polarization dependence, indicating the existence of some degree of ordering of these samples. The existence of spontaneous ordering in nitrogen incorporating GaInP is further confirmed by the HXRC and high resolution transmission electron microscope (HTEM).

Figure 6 shows the HXRC of sample B for [110] and $[1\bar{1}0]$ polarizations. An extra feature adjacent to the $Ga_{0.46}In_{0.54}N_{0.01}P_{0.99}$ peak is detected in the HXRC for the $[1\bar{1}0]$ polarization

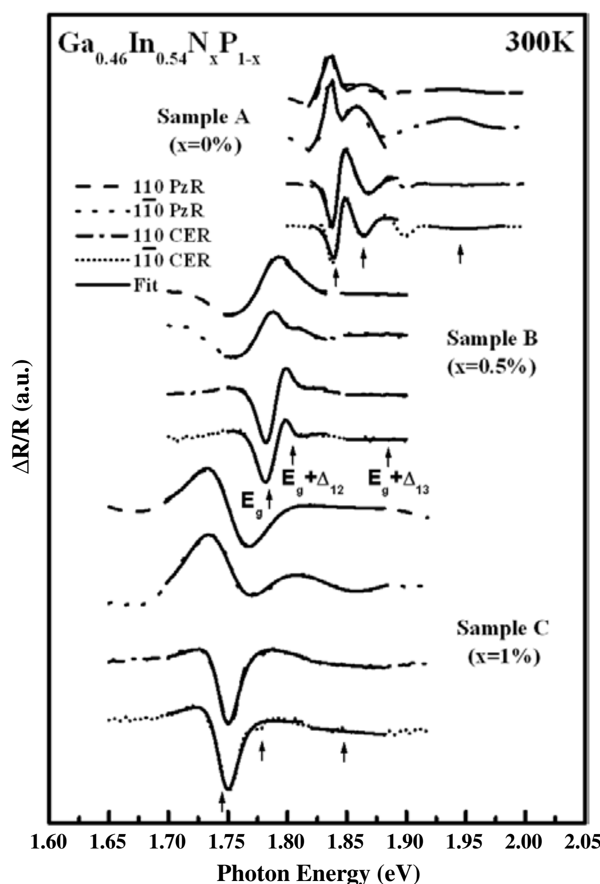

Figure 5. Room temperature polarized CER and PzR spectra of $Ga_{0.46}In_{0.54}N_xP_{1-x}$ epilayers with nitrogen content $x = 0$, 0.5% and 1% in the vicinity of the band edge. The energies of the near band edge critical point transitions E_g, $E_g + \Delta_{12}$ and $E_g + \Delta_{13}$ obtained from the fits are indicated by arrows.

and is not observed for the [110] polarization. The anisotropic properties for the different polarizations can result from either the anisotropic composition fluctuation or spontaneous ordering. However, the results of the SIMS measurements rule out the possibility of anisotropic composition fluctuation. Figure 7 shows the HTEM image taken from sample B ($x = 0.5\%$). The ordering-induced superlattice-like microstructure is seen in this image. It also shows localized clustering and some degree of ordering in the sample.

The polarization dependent dominant features near the band edge correspond to transitions with energy E_g between the top of the valence band and the bottom of the conduction band, and transitions with energy $E_g + \Delta_{12}$ between the crystal field bands and the bottom of the conduction band. The values of E_g, $E_g + \Delta_{12}$ and $E_g + \Delta_{13}$ obtained at room temperature indicated by arrows in figure 5 are listed in table 1. The values of E_g evaluated from PL spectra are also included in table 1. It shows similar results for the determination of the room temperature E_g by modulation spectroscopy and PL measurement. It should be noted that both the epitaxial strain and the atomic ordering induced the valence band splitting, while the strain, ordering and clustering can all lead to a band gap reduction [7]. In order to understand the influence of the nitrogen content in the GaInNP material system, more work needs to be done.

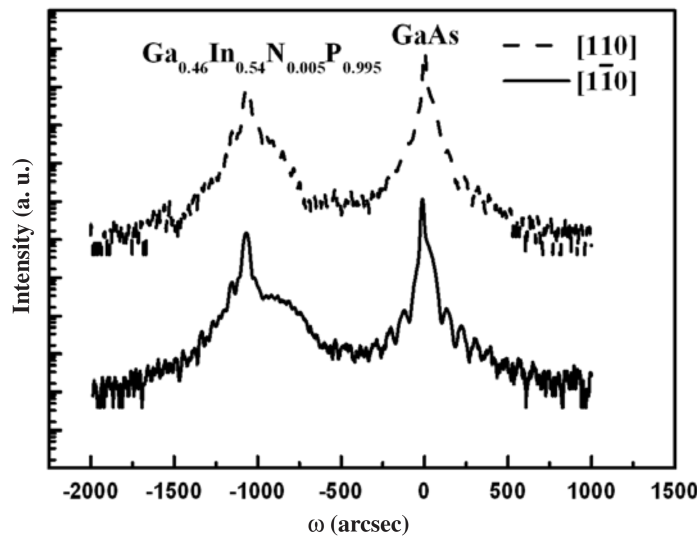

Figure 6. High resolution x-ray rocking curves of $Ga_{0.46}In_{0.54}N_{0.005}P_{0.995}$ for [110] and [1$\bar{1}$0] polarizations.

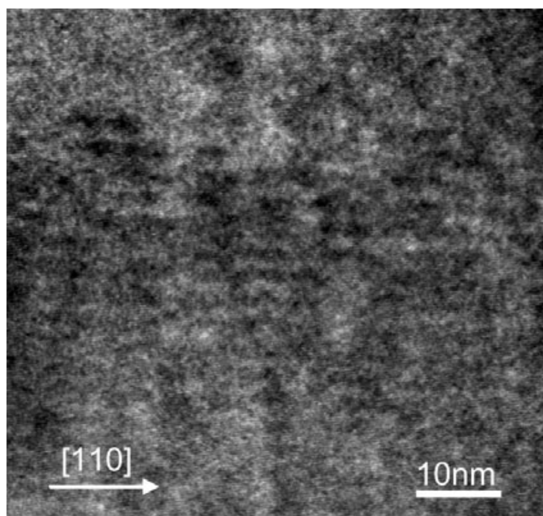

Figure 7. The HTEM images show some degree of ordering and localized clusters in $Ga_{0.46}In_{0.54}N_{0.005}P_{0.995}$ (sample B).

Figures 8 and 9 are the polarized PzR spectra, for **E** ∥ [110] and **E** ∥ [1$\bar{1}$0] respectively, in the vicinity of E_g, $E_g + \Delta_{12}$ and $E_g + \Delta_{13}$ for sample C ($Ga_{0.46}In_{0.54}N_{0.01}P_{0.99}$) at several temperatures between 15 and 300 K. The line shapes of the PzR spectra do not change significantly as a function of temperature. This is in contrast to the PL measurements case, where the low temperature spectra favour the lowest energy transition and emission from the localized states or more ordered domains [23, 24]. Recently Hong *et al* [15] reported a study of the temperature dependence of the PL for $Ga_{0.44}In_{0.56}P$ and $Ga_{0.44}In_{0.56}N_{0.01}P_{0.99}$. For $Ga_{0.44}In_{0.56}N_{0.01}P_{0.99}$, the PL peak energy shows an inverted S-shape in the lower temperature range, while in the higher temperature range the two samples reveal similar temperature

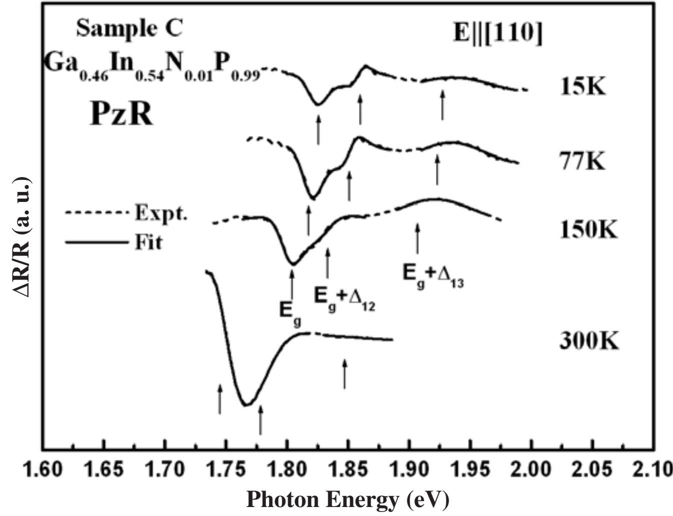

Figure 8. PzR spectra for **E** ∥ [110] for $Ga_{0.46}In_{0.54}N_{0.01}P_{0.99}$ (sample C) at several temperatures between 15 and 300 K. The dashed curves are the experimental curves and the solid curves are least-squares fits to equation (1).

Table 1. The near band edge critical point transition energies E_g, $E_g + \Delta_{12}$ and $E_g + \Delta_{13}$ for $Ga_{0.46}In_{0.54}N_xP_{1-x}$ epilayers with different nitrogen contents at room temperature obtained from CER and PzR measurements. Also included are the band gap energies evaluated from PL spectra.

Samples	E_g [a] (eV)	$E_g + \Delta_{12}$ [a] (eV)	$E_g + \Delta_{13}$ [a] (eV)	E_g [b] (eV)
$Ga_{0.46}In_{0.54}P$	1.840 ± 0.005	1.864 ± 0.005	1.946 ± 0.005	1.826
$Ga_{0.46}In_{0.54}N_{0.005}P_{0.995}$	1.781 ± 0.005	1.803 ± 0.005	1.884 ± 0.005	1.784
$Ga_{0.46}In_{0.54}N_{0.01}P_{0.99}$	1.745 ± 0.005	1.779 ± 0.005	1.848 ± 0.005	1.745

[a] Obtained from CER and PzR.
[b] Obtained from PL.

dependences. The S-shape phenomenon has been attributed to the nitrogen related localized states for the nitrogen incorporating samples.

When the separation between E_g and $E_g + \Delta_{12}$ transitions is less than the experimental linewidth, the usual line-shape fit presents large ambiguity in the determination of the crystal field splitting energy Δ_{12}. We can resolve this difficulty by using polarization selection rules to determine the relative intensity of the two features for both polarizations. These intensity relations have been used in the present fitting procedure to obtain a better estimate of Δ_{12}. The values obtained for E_g, $E_g + \Delta_{12}$ and $E_g + \Delta_{13}$ are indicated by arrows in figures 8 and 9.

The temperature dependences of the E_g, $E_g + \Delta_{12}$ and $E_g + \Delta_{13}$ transitions for samples A, B and C are shown in figure 10. The fitted results for samples A, B and C over the temperature range of 15–300 K are indicated, respectively, by solid circles, solid squares and solid diamonds in figure 10. Representative error bars are shown. From the results shown in figure 10, it is noted that within experimental error, the crystal field splitting Δ_{12} and the spin–orbit splitting Δ_{13} do not depend on temperature. The full curves are the least-squares fits to the Varshni semiempirical relationship [16]:

$$E_{C_i}(T) = E^{V}_{C_i}(0) - \frac{\alpha T^2}{T + \beta}. \tag{2}$$

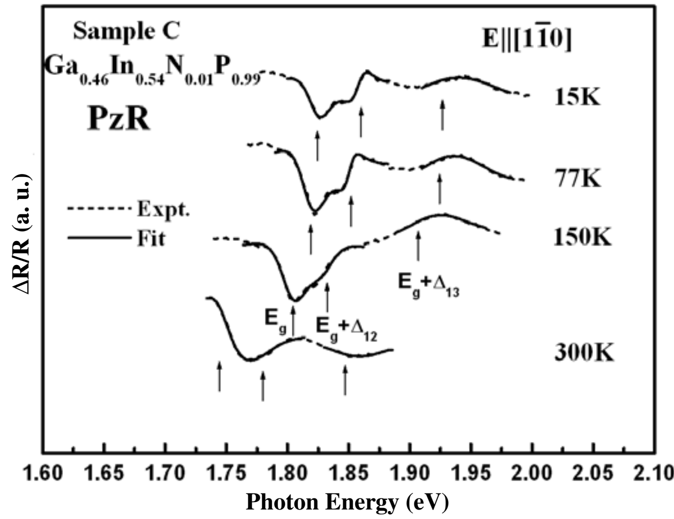

Figure 9. PzR spectra for **E** ∥ [1$\bar{1}$0] for $Ga_{0.46}In_{0.54}N_{0.01}P_{0.99}$ (sample C) at several temperatures between 15 and 300 K. The dashed curves are the experimental curves and the solid curves are least-squares fits to equation (1).

Here, $E^{V}_{C_i}(0)$ is the critical point transition energy (E_g, $E_g + \Delta_{12}$ or $E_g + \Delta_{13}$) at absolute zero; α and β are constants referred to as Varshni coefficients. The constant α is related to the electron–phonon interaction and β is closely related to the Debye temperature [16]. The values obtained for $E^{V}_{C_i}(0)$, α and β for the near band edge critical point transitions for samples A, B and C are listed in table 2.

The temperature dependence of the near band edge critical point transitions of samples A, B and C can also be described by a Bose–Einstein-type expression of the form [17, 18]

$$E_{C_i}(T) = E_{C_i}(0) - \frac{2a_B}{[\exp(\Theta_B/T) - 1]} \qquad (3)$$

where $E_{C_i}(0)$ is the near band edge transition energy at 0 K, a_B represents the strength of the electron–average phonon interaction and Θ_B corresponds to the average phonon temperature. Shown by the dotted curves in figure 10 is a least-squares fit to equation (3). The values obtained for the various parameters are also listed in table 2.

Also included in table 2 are the relevant parameters as determined by fitting the experimental PL spectra for GaInNP [15], PR spectra for GaInNAs/GaAs single quantum wells (SQW) [25] as well as PL and PR spectra for InGaAs/GaAs SQW and GaInNAs/GaAs SQW [26]. From a close examination of the parameters in table 2, we see that the values of α and β depend on the measurement technique. It seems that most of the values of α and β from other works fall below 0.6 meV K^{-1} and 400 K, respectively, except that of [14] obtained by Hong *et al* where the PL measurement technique is used. However, low temperature PL spectra were reported to be a rather poor technique for the determination of the band gap of the dilute nitride compounds, since for PL measurement at low temperature, there is a selective preference for the transition from the lowest level localized state [27]. Hence the values extracted from PL measurements of [14] may not be reliable in comparing with the other measurement techniques.

The parameter α of equation (2) can be related to a_B and Θ_B of equation (3) by taking the high temperature limits of both expressions. This yields $\alpha = 2a_B/\Theta_B$. Comparison of the

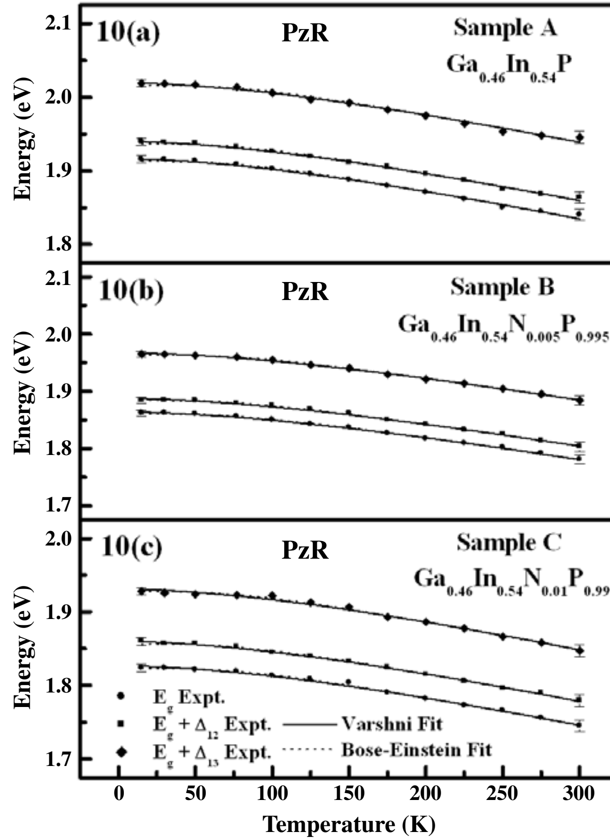

Figure 10. The temperature variations of E_g, $E_g + \Delta_{12}$ and $E_g + \Delta_{13}$ for (a) $Ga_{0.46}In_{0.54}P$ (sample A), (b) $Ga_{0.46}In_{0.54}N_{0.005}P_{0.995}$ (sample B) and (c) $Ga_{0.46}In_{0.54}N_{0.01}P_{0.99}$ (sample C) with representative error bars. The solid curves are least-squares fits to the Varshni-type semiempirical relationship and the dotted curves are fitted to the Bose–Einstein-type expression.

numbers shown in table 2 shows that this relation is indeed satisfied. The temperature shift of the interband transition energies is mainly due to the interactions of electron with the relevant acoustic and optical phonons. According to the existing theory this leads to a value of Θ_B significantly smaller than the average LO phonon temperature Θ_{LO}. The value of $\Theta_{LO} \approx 530$ K is deduced from the Raman spectra of $Ga_{0.48}In_{0.52}P$ [28, 29]. From table 2, it can be seen that our fitted values of Θ_B showed this theoretical trend. It is also noted that the parameters obtained that describe the temperature variation of the transition energies are quite similar for the nitrogen incorporating and nitrogen free samples. These results are quite at variance with other reports that nitrogen incorporation can reduce the dependence of the transition energy on temperature [15, 30]. However, our results agreed well with the those reported by Shirakata *et al* [26]. The Shirakata *et al* study of GaInAs/GaAs and GaInNAs/GaAs SQW using temperature dependent PL and PR showed comparable temperature coefficients of the fundamental transition energy for GaInAs and GaInNAs SQW in the high temperature region 160 K $\leqslant T \leqslant$ 300 K (-3.48×10^{-4} versus -3.35×10^{-4} eV K^{-1}). The results indicate that the influence of nitrogen incorporation mainly shows up in the lower temperature region where localized states are created by the presence of nitrogen. However, at higher temperature, these

Table 2. Values of the Varshni-type and Bose–Einstein-type fitting parameters, which describe the temperature dependence of the near band edge critical point transition energies of $Ga_{0.46}In_{0.54}N_xP_{1-x}$, $Ga_{0.44}In_{0.56}N_xP_{1-x}$, and the fundamental transition energy E_{11H} of GaInNAs/GaAs SQW and GaInAs/GaAs SQW.

Samples	Feature	$E^{V}_{C_i}(0)$ (eV)	α (meV K^{-1})	β (K)	a_B (meV)	Θ_B (K)	Temperature range (K)
$Ga_{0.46}In_{0.54}N_xP_{1-x}$ ($x = 0$)	E_g[a]	1.914 ± 0.005	0.49 ± 0.05	250 ± 50	53 ± 15	255 ± 50	15–300
	$E_g + \Delta_{12}$[a]	1.938 ± 0.005	0.49 ± 0.05	250 ± 50	52 ± 15	255 ± 50	
	$E_g + \Delta_{13}$[a]	2.018 ± 0.005	0.49 ± 0.05	250 ± 50	52 ± 15	255 ± 50	
$Ga_{0.46}In_{0.54}N_xP_{1-x}$ ($x = 0.005$)	E_g[a]	1.862 ± 0.005	0.51 ± 0.05	255 ± 50	53 ± 15	250 ± 50	15–300
	$E_g + \Delta_{12}$[a]	1.886 ± 0.005	0.51 ± 0.05	255 ± 50	52 ± 15	250 ± 50	
	$E_g + \Delta_{13}$[a]	1.966 ± 0.005	0.51 ± 0.05	255 ± 50	52 ± 15	250 ± 50	
$Ga_{0.46}In_{0.54}N_xP_{1-x}$ ($x = 0.01$)	E_g[a]	1.825 ± 0.005	0.49 ± 0.05	255 ± 50	53 ± 15	250 ± 50	15–300
	$E_g + \Delta_{12}$[a]	1.858 ± 0.005	0.50 ± 0.05	255 ± 50	51 ± 15	250 ± 50	
	$E_g + \Delta_{13}$[a]	1.929 ± 0.005	0.50 ± 0.05	255 ± 50	52 ± 15	250 ± 50	
$Ga_{0.44}In_{0.56}N_xP_{1-x}$ ($x = 0$)	E_g[b]	1.866	1	1475			10–300
$Ga_{0.44}In_{0.56}N_xP_{1-x}$ ($x = 0.01$)	E_g[c]		1	1475			150–300
GaInNAs/GaAs SQW	E_{11H}[d]	0.950	0.59	300			10–300
GaInNAs/GaAs SQW	E_{11H}[e]	1.05	0.55	384			8–300
GaInAs/GaAs SQW	E_{11H}[f]	1.17	0.6	376			8–300

[a] Present work (polarized piezoreflectance).
[b] Reference [14] (photoluminescence).
[c] Reference [14] (photoluminescence) exhibits an inverted S-shape dependence with temperature $T \leqslant 150$ K.
[d] Reference [25] (photoreflectance).
[e] Reference [26] (photoreflectance).
[f] Reference [26] (photoluminescence).

localized states can be completely activated and the temperature coefficient of the transition energy becomes similar to that of the nitrogen free compounds.

4. Summary

A detailed structural and optical characterization of $Ga_{0.46}In_{0.54}N_xP_{1-x}$ epilayers has been carried out. The anisotropic properties of the polarized high resolution x-ray rocking curves, CER and PzR spectra along the [110] and [$1\bar{1}0$] directions as well as the ordering-induced superlattice-like microstructure observed in HTEM images reveal spontaneous ordering in $Ga_{0.46}In_{0.54}N_xP_{1-x}$ layers. In addition, the temperature dependent optical properties have been studied by using polarized PzR measurements in the range between 15 and 300 K. The PzR spectra obtained have been fitted via a theoretical functional form and the valence band maximum, crystal field/strain splitting and spin–orbit splitting to conduction band transition energies, denoted as E_g, $E_g + \Delta_{12}$ and $E_g + \Delta_{13}$, respectively, which have been accurately determined. The temperature dependences of these near band edge critical point transition energies are analysed using the Varshni expression and an expression containing the Bose–Einstein occupation factor for phonons. The parameters that describe the temperature variation of the transition energies have been evaluated and found to be insensitive to the nitrogen content.

Acknowledgments

The authors acknowledge the support of the National Science Council of Taiwan. C H Wu and Y K Su acknowledge the support of the Ministry of Education, Taiwan, under the Programme for Promoting Academic Excellence of Universities project No A-91-E-FA08-1-4.

References

[1] Liau Z L, Palmateer S C, Groves S H, Walpole J N and Missaggia L J 1992 *Appl. Phys. Lett.* **60** 6
[2] Katsuyama T, Yoshida T, Shinkai J, Hashimoto J and Hayashi H 1991 *Appl. Phys. Lett.* **59** 3351
[3] Yow H Y, Houston P A, Button C C, Lee T W and Roberts S J 1994 *J. Appl. Phys.* **76** 8135
[4] Yang Y F, Hsu C C and Yang E S 1996 *IEEE Electron Device Lett.* **17** 363
[5] Bertness K A, Kurtz S R, Friedman D J, Kibbler A E and Olson J M 1994 *Appl. Phys. Lett.* **65** 989
[6] Gomyo A, Suzuki T and Iijima S 1988 *Phys. Rev. Lett.* **60** 2645
[7] Wei S H and Zunger A 1994 *Phys. Rev.* B **49** 14337
[8] Ernst P, Geng C, Scholz F, Schweizer H, Zhang Y and Mascarenhas A 1995 *Appl. Phys. Lett.* **67** 2347
[9] Kressel H, Nuese C I and Ladany I J 1973 *J. Appl. Phys.* **44** 3266
[10] Perkins J D, Mascarenhas A, Zhang Y, Geisz J F, Friedman D J, Olson J M and Kurtz S R 1999 *Phys. Rev. Lett.* **82** 3312
[11] Yu K M, Walukiewicz W, Wu J, Beeman J W, Ager J W III, Haller E E, Shan W, Xin H P and Tu C W 2001 *Appl. Phys. Lett.* **78** 1077
[12] Shan W, Walukiewicz W, Yu K M, Wu J, Ager J W III, Haller E E, Xin H P and Tu C W 2000 *Appl. Phys. Lett.* **76** 3251
[13] Welty R J, Hong Y G, Xin H P, Mochizuki K, Tu C W and Asbeck P M 2000 *Proc. 2000 IEEE/Cornell Conf. on High Performance Devices (Piscataway, USA)* (Piscataway, NJ: IEEE) p 33
[14] Hong Y G, Juang F S, Kim M H and Tu C W 2003 *J. Cryst. Growth* **251** 437
[15] Hong Y G, André R and Tu C W 2001 *J. Vac. Sci. Technol.* B **19** 1413
[16] Varshni Y P 1967 *Physica* **34** 149
[17] Lantenschlager P, Garriga M, Logothetidis S and Cardona M 1987 *Phys. Rev.* B **35** 9174
[18] Viña L, Logothetidis S and Cardona M 1984 *Phys. Rev.* B **30** 1979
[19] Pollak F H and Shen H 1993 *Mater. Sci. Eng.* R **10** 275
[20] Tu C W, Bi W G, Ma Y, Zhang J P, Wang L W and Ho S T 1998 *IEEE J. Sel. Top. Quantum Electron.* **4** 510
[21] Baillargeon J N, Cheng K Y, Hofler G E, Pearah P J and Hsieh K C 1992 *Appl. Phys. Lett.* **60** 2540
[22] Bi W G and Tu C W 1997 *Appl. Phys. Lett.* **70** 1608
[23] Kanata T, Nishimoto M, Nakayama H and Nishino T 1992 *Phys. Rev.* B **45** 6637
[24] Delong M C, Mowbray D J, Hogg R A, Skolnick M S, Hopkinson M, David J P R, Taylor P C, Kurtz S R and Olson J M 1993 *J. Appl. Phys.* **73** 5163
[25] Grenouillet L, Bru-Chevallier C, Guillot G, Gilet P, Duvaut P, Vannuffel C, Million A and Chenevas-Paule A 2000 *Appl. Phys. Lett.* **76** 2241
[26] Shirakata S, Kondow M and Kitatani T 2001 *Appl. Phys. Lett.* **79** 54
[27] Yu P Y and Cardona M 1996 *Fundamentals of Semiconductors* (Berlin: Springer)
[28] Kondow M, Minagawa S and Satoh S 1987 *Appl. Phys. Lett.* **51** 2001
[29] Cheong H M, Mascarenhas A, Ernst P and Geng C 1997 *Phys. Rev.* B **56** 1882
[30] Rudko G Y, Buyanova I A, Chen W M, Xin H P and Tu C W 2002 *Appl. Phys. Lett.* **81** 3984